

# X ray and visible light transmission for laboratory measurement of two-dimensional saturation fields in thin-slab systems

Vincent C. Tidwell and Robert J. Glass

Geohydrology Department, Sandia National Laboratories, Albuquerque, New Mexico

**Abstract.** Two independent techniques, X ray absorption and light transmission, are developed and demonstrated for imaging transient saturation fields in thin-slab porous systems. The techniques yield full two-dimensional saturation fields with high spatial and temporal resolution. In the time required to make a single measurement by one of the traditional methods (e.g., gravimetric or gamma densitometry) an entire image consisting of hundreds of thousands of points is acquired by either the X ray or light technique. These methods are also very sensitive, capable of resolving a hundred or more levels of saturation at each of these points. Evaluation of these techniques is accomplished by direct comparison of X ray and light data as well as comparison with gravimetric and gamma densitometry data. Results of the comparison show very close agreement between the four techniques (on average within 5% saturation). These techniques represent useful tools for investigating processes governing unsaturated flow and transport through porous media.

## 1. Introduction

Hypothesis testing for flow in unsaturated porous media is limited by the ability to measure dependent variables in heterogeneous and/or transient systems. Recently, a number of tools for nonintrusive measurement of water saturation in the laboratory have been developed beyond the standard gamma densitometer [Gardner, 1982]. Examples include computed tomography (CT) [Crestana *et al.*, 1985; Anderson *et al.*, 1988], nuclear magnetic resonance (NMR) [Matzkanin and Paetzold, 1982], electromagnetic tomography [Daily and Ramirez, 1989], and microwave attenuation [Latorre and Glenn, 1991]. Each of these methods for measuring saturation within laboratory test cells is limited in spatial or temporal resolution or in size of the sample, or requires very specialized and expensive equipment.

In this paper, we explore two alternative laboratory techniques, X ray absorption (film-based radiography) and visible light transmission [e.g., Glass *et al.*, 1989a]. These techniques are developed for use in thin but extensive experimental systems. The two methods rely on the transmission of either X rays or visible light through the test system (incident rays oriented normal to slab plane). The transmitted X ray or light intensity field is recorded by means of digital imaging equipment. Analysis of the resulting images yields two-dimensional saturation fields (integrated across the thickness of the slab) at high spatial and temporal resolution.

We present a brief overview of the X ray and light transmission techniques and the theoretical basis for each. We then present the results of an experimental program designed to compare the techniques with standard gravimetric and gamma densitometry methods. Results of the comparison show very close agreement (on average within 5% saturation) between the X ray, light, gamma, and gravimetric

data. Comparison of repeated measurements show similar results for the precision of X ray and light imaging.

## 2. Methods

With both the X ray and light techniques, electromagnetic energy is passed through the test media and the liquid saturation distribution integrated over the media's thickness is measured as variations in the transmitted X ray or light intensity field. The difference between the techniques lies in the frequency of the radiation used and in the physics governing the interaction that gives rise to variations in the transmitted intensity field. When using low energy X rays (below 75 keV), variations in the transmitted intensity field arise from the sensitivity of X ray absorption (photoelectric absorption) to the density of the media, which is directly related to liquid saturation (i.e., increase in saturation yields a decrease in X ray transmission). For the light technique an increase in saturation results in an increase in light transmission because of the closer matching of the index of refraction of the matrix and water relative to the matrix and air.

### 2.1. Measurement Techniques

X ray images are acquired by directing a beam of X rays at the face of the test media while recording the transmitted intensity field on film secured behind the test chamber (Figure 1). The exposed film is developed and then placed in front of a diffused bank of high-frequency (60 Mhz), high-output fluorescent lights for digital imaging. Care must be taken in selecting the light source if video equipment is used in imaging. For this application, the frequency of the light source must be selected to be different than the frequency of the video equipment. A reasonably constant light source intensity level is also required; in our system, light output from the fluorescent light bank is controlled through a feedback circuit. Variation in the transmitted light intensity field is recorded by means of a CCD (charge-coupled device) camera focused on the front of the film. At present, camera output is digitized into an array of 512 by 512 points (a total

This paper is not subject to U.S. copyright. Published in 1994 by the American Geophysical Union.

Paper number 94WR00953

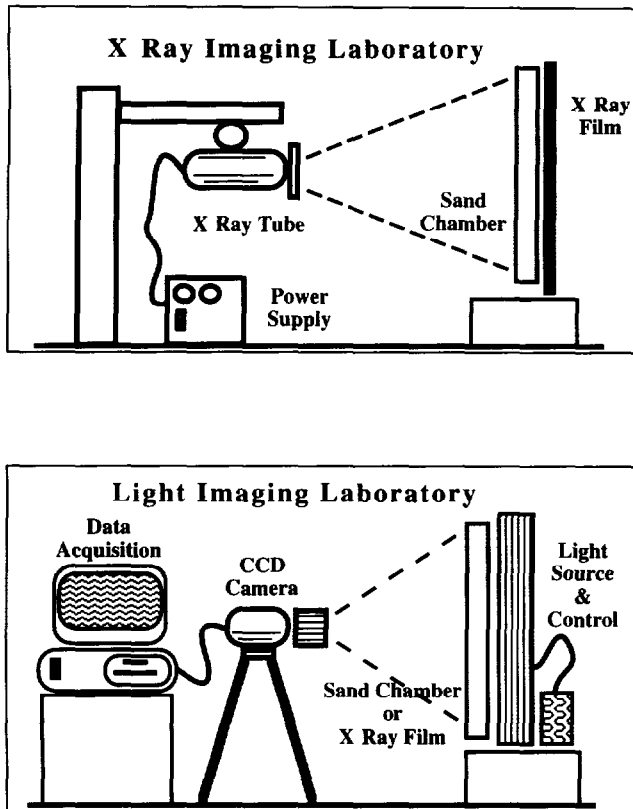


**Figure 1.** Schematic of the X ray and light imaging laboratories. Note that the distance between the CCD camera and focal plane is much larger than that depicted to minimize parallax-induced error.

of 262,144 points), with each point assigned a grey level between zero and 255 according to the transmitted light intensity; however, greater resolution in grey scale can be achieved with more sophisticated digital cameras. The spatial resolution of the acquired image is defined by the array size of the camera and the size of the test system. For the studies described in this paper, images are acquired at a resolution of 8.4 data points per centimeter.

For the light transmission technique, introduced qualitatively by Glass *et al.* [1989a], imaging is accomplished identically to that for the X ray film, where the test chamber is simply exchanged with the X ray film (Figure 1). Transmitted light images are collected as the experiment proceeds at a temporal resolution of 30 images per second (temporal resolution is a function of the equipment used).

Digitized grey level values are converted to water saturation through a two-step process, discussed in detail below. The first step adjusts the image to correct for variations in the imaging source intensity and variations in film quality. In the second step, the adjusted grey level values are converted to saturation through a functional relationship based on either X ray absorption or light refraction theory.

## 2.2. Image Adjustments

Image adjustment for the light technique is required to correct for variations in the light source intensity. Adjustments to X ray images also are required for this reason, as well as to correct for variations in image density resulting from temperature and time fluctuations in the film develop-

ment process and differences in film emulsion. Image adjustment is accomplished in the same manner for both the X ray and light techniques. A variable density wedge is incorporated into each of the X ray and light images. The wedge covers the complete density range, thus providing a constant scale within each image by which adjustment can be accomplished. A curve is fit to the grey level/wedge density relationship for each image. An adjustment function is then fit to map the curves for each of the images to that of a selected reference image. Grey level values across the entire image then are corrected using the adjustment function.

## 2.3. Saturation Calculation: X Ray Transmission

The mapping of X ray intensity (recorded as digitized grey level data) to pointwise saturation values is predicated on X ray absorption theory [Brown, 1966; Kaelble, 1967]. For a well-collimated beam of monochromatic X rays, Lambert's law predicts an exponential decrease in X ray intensity with distance traversed through the material.

$$I_X = I_{X0} \exp(-\rho\mu x) \quad (1)$$

where  $I_X$  is the transmitted X ray intensity,  $I_{X0}$  is the incident X ray intensity,  $\mu$  is the mass absorption coefficient, and  $\rho$  and  $x$  are the bulk density and thickness of the medium, respectively. For a three-phase system composed of porous material, liquid, and test chamber glass (air is neglected owing to its low absorption characteristics), Equation (1) becomes

$$I_X = I_{X0} \exp[-(\rho_s\mu_s x + \rho_l\mu_l x + 2T\rho_c\mu_c)] \quad (2)$$

where  $T$  is the thickness of the chamber wall;  $\rho_s$ ,  $\rho_l$ , and  $\mu_c$  are the mass absorption coefficients for the porous media, liquid, and chamber, respectively.

Equations (1) and (2) assume a monochromatic X ray source; however, industrial and medical radiography equipment emit a polychromatic X ray beam. For a polychromatic source, X ray absorption becomes nonlinear owing to the preferential absorption of low-energy X rays. To account for this nonlinear behavior would require a significant amount of information, which for most practical purposes is impossible to acquire. Here we assume that Lambert's law provides a first-order approximation for the absorption process. This assumption should be reasonable because the chamber and porous material act as a filter, preferentially absorbing the low-energy X rays. The result of such filtering leaves a relatively narrow (approaching monochromatic) X ray spectrum for imaging.

Because the transmitted X ray intensity is recorded on film, a relationship between film exposure  $E$  and the transmitted X ray intensity  $I_X$  is required:

$$I_X = E/t \quad (3)$$

where  $t$  is the exposure time. The film exposure is related to transmitted light intensity  $I_v$  (as measured by the video camera and quantified in terms of grey level) through the relationship

$$E = E_0(I_{v0}/I_v)^{1/\gamma} \quad (4)$$

where  $E_0$  is the saturation point of the exposure,  $\gamma$  is the slope of the film emulsion characteristic curve, and  $I_{v0}$  is the

intensity of the light incident on the X ray film. Combining (3) and (4) and substituting into (2) yields

$$\ln [E_0(I_{v0}/I_v)^{1/\gamma}] - \ln [I_{x0}t] = -(\rho_s \mu_s x + \rho_l \mu_l x + 2T\rho_c \mu_c) \quad (5)$$

Equation (5) quantifies the relationship between fluid content (i.e.,  $\rho_l$ ) and digitized grey level at any point in the test media. Equation (5) may be simplified by subtracting the influence of the porous media and chamber (captured in the dry image) and scaling the resulting expression by the difference between the fully saturated and dry image. The resulting expression provides a simple means of calculating saturation  $S$  at each point in the thin slab.

$$S = \frac{\ln(I_v) - \ln(I_{vd})}{\ln(I_{vs}) - \ln(I_{vd})} \quad (6)$$

$I_{vd}$  and  $I_{vs}$  are the point grey level values for dry and saturated conditions, respectively.

#### 2.4. Saturation Calculation: Light Transmission

Visible light transmission was first used quantitatively by *Hoa* [1981] to measure the saturation within a thin, sand-filled slab chamber using a small, movable light transmission sensor. His theoretical development may be applied directly within our context, as described below.

Light that passes through the porous media encounters sand, air, and water. Through each of these phases, light is absorbed exponentially as discussed above for X rays. In addition, as light passes a phase interface (air-water, sand-air, sand-water) it is scattered and refracted, the transmitted intensity of the passing light being a function of the refractive indices of the two phases and the angle of incidence (micro-scale geometry). Assuming normal incidence, the ratio of emergent to incident light, referred to as the light transmission factor  $\tau$ , is given by Fresnel's Law:

$$\tau = 4n/(n+1)^2 \quad (7)$$

where  $n$  is the ratio of refractive indices of the two phases. With the refractive indices of sand, water, and air (1.6, 1.33, and 1.0, respectively),  $\tau_{sw}$  for the sand-water interface and  $\tau_{sa}$  for the sand-air interface are calculated to be 0.991 and 0.946, respectively. Thus if sand-water interfaces replace sand-air interfaces, emergent light intensity will increase.

If we assume that each individual pore is either full or empty of water, then the intensity of light transmitted across the system,  $I_v$ , is given by

$$I_v = I_{vd} \exp [-(K_s - K_a)d_w](\tau_{sw}/\tau_{sa})^{2p} \quad (8)$$

where  $I_{vd}$  is the emergent light intensity for the dry sample,  $K_s$  and  $K_a$  are the light absorption moduli of water and air, respectively,  $d_w$  is the sum thickness of water-filled pores, and  $p$  is the number of pores filled with water. Since the difference between  $K_s$  and  $K_a$  is very small, we can approximate (8) with

$$I_v = I_{vd}(\tau_{sw}/\tau_{sa})^{2p} \quad (9)$$

Application of (9) to calculate moisture content or saturation requires two additional steps. First, inhomogeneities in the lighting (mostly edge effects) and recording systems (sensor field) that do not result from moisture content must

be removed. This is accomplished through the standard normalization procedure defining the normalized light intensity  $I_{vn}$ , at a point

$$I_{vn} = (I_v - I_{vd})/(I_{vs} - I_{vd}) \quad (10)$$

where  $I_{vd}$  and  $I_{vs}$  are the emergent light intensities for the dry and saturated conditions, respectively. Second, a relationship between the number of pores filled with water,  $p$ , and the moisture content or saturation must be found. *Hoa* [1981] argued that the relationship between  $p$  and the moisture content is unknown and so developed an independent empirical calibration curve between emergent intensity and saturation. In principle, however, the relation between  $p$  and the moisture content could be calculated from the moisture characteristic curve and capillary tube theory. Here, as a first step in seeking a simple functional mapping with physical significance, we make the assumption that

$$p = Sk \quad (11)$$

where  $S$  is the saturation and  $k$  is the average number of pores across the sample. Substituting (9) and (11) into (10) and solving for  $S$  yields

$$S = \frac{\ln [I_{vn}[(\tau_{sw}/\tau_{sa})^{2k} - 1] + 1]}{2k \ln [\tau_{sw}/\tau_{sa}]} \quad (12)$$

In principle, the average number of pores across the sample may be calculated from geometric arguments for regular or random packings. Another approach, used here, is to choose  $k$  to match the simplest, most readily available data for a given experiment. In this way,  $k$  becomes an empirically measured parameter. We chose  $k$  to the nearest whole number by approximately matching the average volumetric moisture content integrated over the entire chamber with the measured average volumetric moisture content (measured by gravimetric means, water in minus water out of the chamber) at the end of the first drainage cycle (described below).

#### 2.5. Technique Limitations

The measurement of saturation with either technique requires achievement of suitable image contrast. Contrast is defined here as the difference between the intensity field transmitted through the saturated test media to that transmitted through the dry test media. Image contrast is governed both by the physics of the techniques, as discussed above, and the measurement system (film, CCD camera). For a given measurement system, contrast may be optimized by design of the fluid-porous media system. For the X ray technique, difficulty arises because of the low density of water relative to that of the minerals composing the porous media; hence a large change in saturation produces only a small decrease in transmitted X ray intensity. Theory indicates that image contrast may be improved by increasing the thickness of the media and/or decreasing the keV of the X ray source [*Kravchuk and Strashkevich*, 1973]; however, the extent to which these parameters may be adjusted is limited by the sensitivity of the X ray detecting device. Another alternative for increasing contrast, which we employ here, involves doping the water with a contrast enhancing agent. The iodine ion, added in the form of potassium iodide (KI),

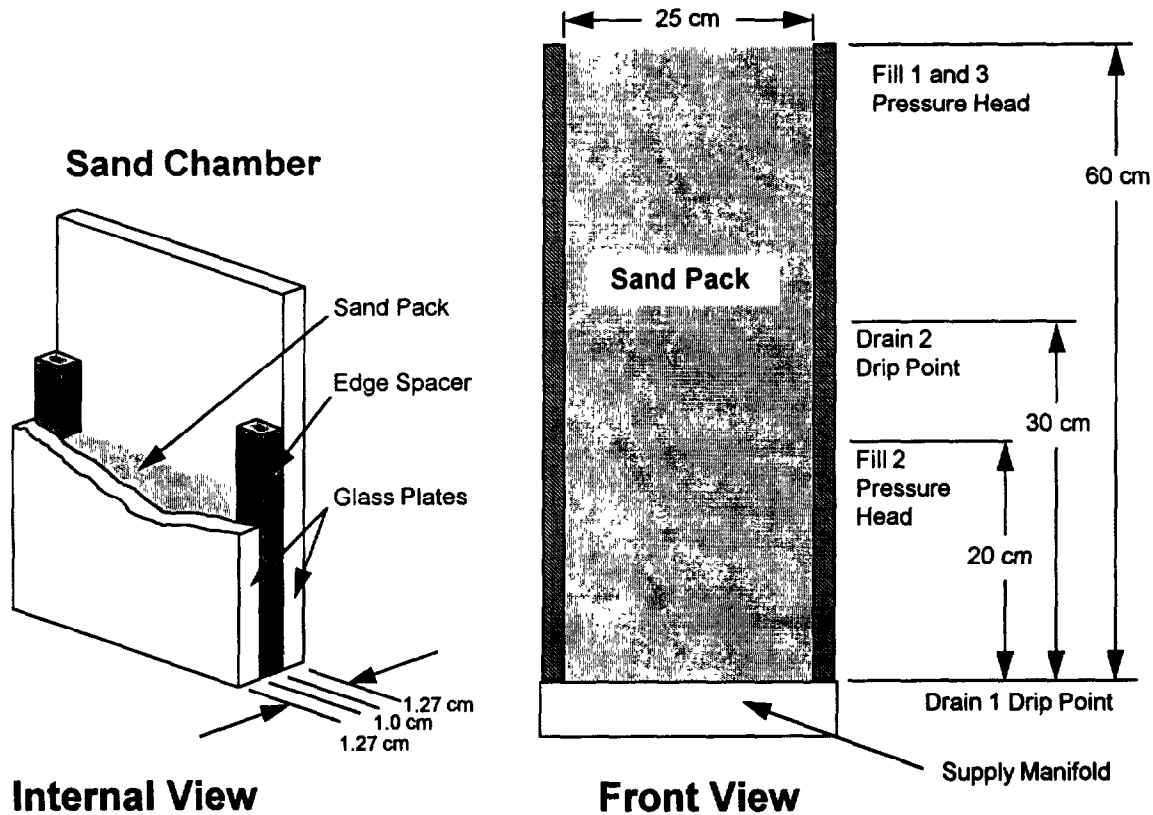


Figure 2. Schematic of the sand chamber used in comparison studies.

is used as it is a conservative tracer and possesses favorable X ray absorption characteristics. A 10% solution (by weight) was used in these studies; however, solution strength may be decreased if an associated decrease in image contrast can be tolerated. It should be noted that the addition of KI will influence fluid properties (i.e., density, surface tension) and hence the suitability of the KI solution as a surrogate for water must be evaluated on a case-by-case basis.

For the transmitted light technique, image contrast is governed by differences in the refractive indices of the air-sand and fluid-sand interfaces. In the air-water-sand systems of interest here, contrast is exceptional without modification. However, it must be recognized that the application of the light technique requires that the porous media be translucent (i.e., silica sands, glass beads), and thus the thickness of the test media is limited (on the order of a centimeter for most cases).

### 3. Comparison Experiments

The X ray and light transmission techniques are compared with each other and with gravimetric and gamma densitometry techniques through a series of experiments conducted in a thin, vertically oriented slab chamber (25 cm wide by 60 cm tall by 1 cm thick) (Figure 2). Three separate tests were performed using three silica sands, 0.42–0.30 mm, 0.59–0.21 mm, and 0.84–0.149 mm, each differing only in their distributions about a common mean grain size. To achieve a homogeneous sand pack, the method of Glass *et al.* [1989b] was used to fill the slab chamber. Each sand was subjected

to three wetting and two drainage sequences using a 10% (by weight) KI solution. Each sequence was initiated with a change in boundary condition.

For “fill 1,” starting in the initially dry condition, the chamber was filled from the bottom to saturation with 0 pressure head at the top and 60 cm at the bottom. For “drain 1” the pressure head at the bottom of the chamber was decreased to 0 cm, and the chamber was drained slowly to equilibrium. For “fill 2” the pressure head at the bottom of the chamber was increased to 20 cm, and the chamber was filled slowly to equilibrium. For “fill 3” the pressure head at the bottom of the chamber was increased to 60 cm, and the chamber was filled slowly to equilibrium. For “drain 2” the pressure head at the bottom of the chamber was decreased to 30 cm, and the chamber was drained slowly to equilibrium.

Transmitted light images were collected to follow the transient moisture changes within the chamber while the mass of water added to and drained from the chamber was monitored with time. Before fill 1 (dry chamber) and after the chamber had reached equilibrium (at least 12 hours) following fill 1, drain 1, fill 2, and drain 2, the chamber was moved to the X ray facility and then to the gamma facility to image the steady liquid saturation fields. Because of the time required to image the chamber using the gamma densitometer (approximately 4 hours), gamma data were collected for the 0.42- to 0.30-mm sand only.

A Philips model 420 industrial X ray unit was used in the experiments described in this paper. X ray images were acquired using a tube potential of 60 kV, a tube current of 15 mA, and an exposure time of 10.25 min (the long exposure

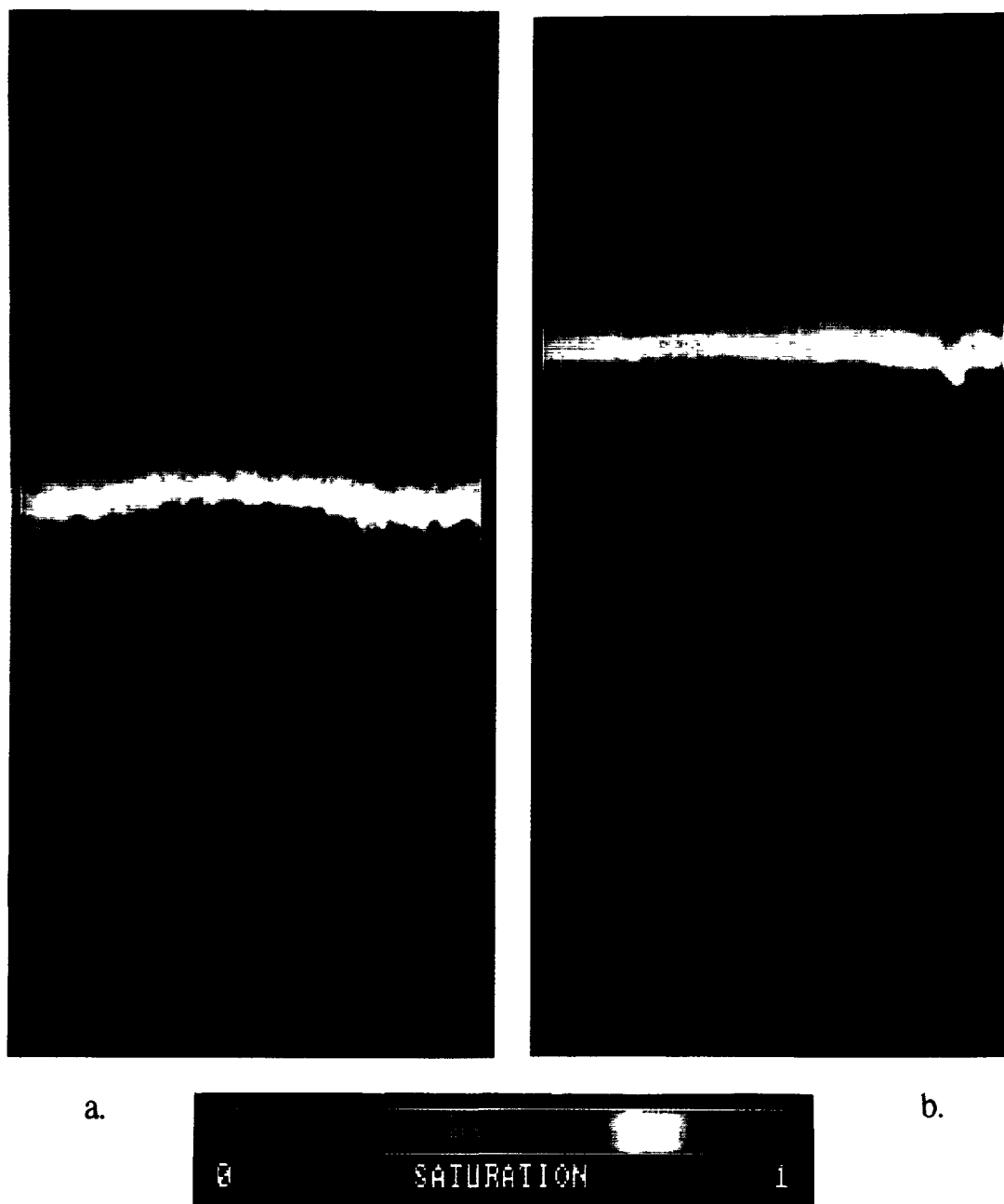


**Plate 1.** Example of images used in the comparison studies. Shown are (a) X ray image of the drain 1 series, and (b) light image for the fill 2 series; both for the 0.42- to 0.30-mm sand. Note the detail in the saturation fields, particularly in areas of high saturation contrast.

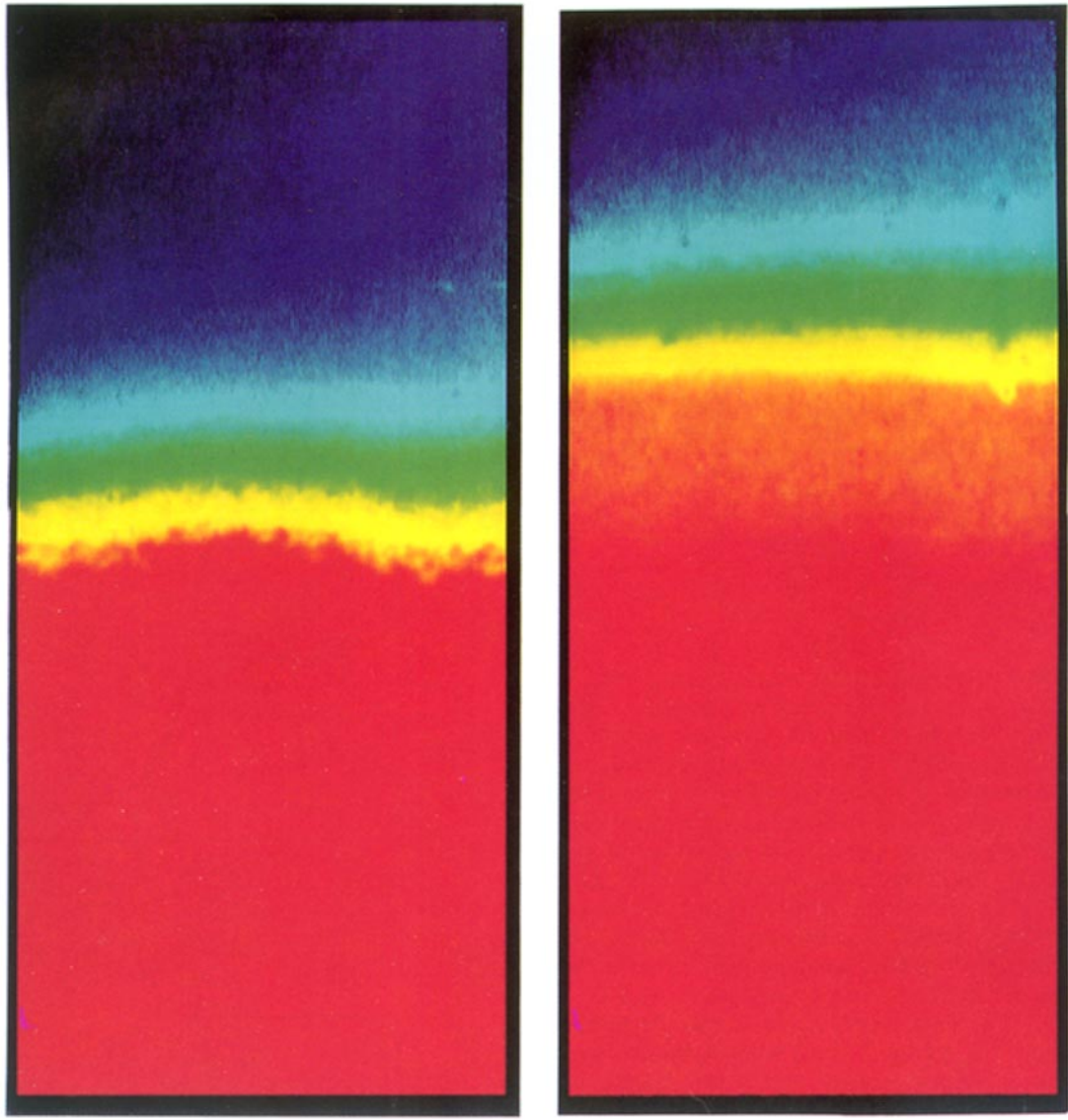
time is due to the thick glass used in the construction of the sand chamber). The source-to-sample distance was maintained at 2.5 m while the 1.27-cm-thick chamber glass defined the sample-to-film distance.

Gamma densitometry measurements were made with a 0.5-Ci cesium 137 source and measured by means of a collimated NaI scintillation detector. Critical measurement parameters include a 0.31-cm detector aperture, and a 30-s count time. Measurements were made at 1.0-cm spacings along vertical transects moving from bottom to top of the sand chamber (total of 60 measurements). A total of five

transects were made near the middle of the chamber, spaced 1.0 cm apart.

#### 4. Results of Comparison Experiments

Comparisons between the X ray, light, gamma, and gravimetric methods are carried out at the drain 1, fill 2, and drain 2 equilibrium conditions for each of the three sands tested. Plate 1 shows an example of a drain 1 and fill 2 saturation field used in the comparison studies. Three different comparisons were made, progressing from the lowest to highest



a.



b.

**Table 1.** Total Volume of Water in Chamber as Measured by the Gravimetric, X ray, Light, and Gamma Techniques

Sequence	Gravimetric	X Ray	Visible Light	Gamma
<i>0.42- to 0.30-mm Sand (Porosity = 0.3916, <math>\theta = 0.3818</math>, <math>k = 19</math>)</i>				
Drain 1	325.7	328.7	329.6	327.0
Fill 2	392.9*	413.0	412.9	396.3
Drain 2	389.2*	406.6	405.4	388.7
<i>0.59- to 0.21-mm Sand (Porosity = 0.3817, <math>\theta = 0.3625</math>, <math>k = 21</math>)</i>				
Drain 1	306.3	308.1	309.3	...
Fill 2	420.1	426.6	426.3	...
Drain 2	403.8	407.6	405.7	...
<i>0.84- to 0.149-mm Sand (Porosity = 0.3688, <math>\theta = 0.3482</math>, <math>k = 33</math>)</i>				
Drain 1	352.0	347.6	347.6	...
Fill 2	407.9	407.9	410.1	...
Drain 2	432.6	438.4	436.4	...

Here  $k$  is the average number of pores across the sample, and  $\theta$  is saturated moisture content. Values are reported in milliliters.

\*Error in mass balance due to storage change during water injection after drain 1.

degree of spatial resolution: (1) the total volume of water in the chamber, (2) the average saturation profile with chamber height, and (3) the direct point-by-point comparison of saturation fields measured by the X ray and light techniques.

Our first comparison, based on the total volume of water within the chamber (Table 1), shows good agreement among all four of the independent methods. In general, deviations from the measured gravimetric data are less than 3% of the total volume of water in the chamber, while differences between the X ray and light data are even less. It should be noted that difficulties were encountered with the collection of the gravimetric data, especially in the case of the 0.42- to 0.30-mm sand, due to air entrapment within the bottom supply manifold that occurred during filling of the chamber. This may account for discrepancies of the order of 2% of the total volume of water in the chamber.

Our second comparison explores average saturation as a function of chamber height. Profiles for the drain 1 and fill 2 series for each of the sands are presented in Figure 3; the drain 2 profiles have been excluded simply for the sake of clarity. Each point in Figure 3 is an arithmetic average for all points at that height in the chamber (235 points for the X ray and light techniques, and 5 points for the gamma densitometer). The X ray and light data are taken at a height resolution of 8.4 data points per centimeter, while the gamma densitometer data are collected at a resolution of one data point per centimeter with a detection aperture of 0.31 cm (i.e., only 0.31 cm of the 1.0-cm interval is measured). We note again that gamma densitometer data were collected for the 0.42- to 0.30-mm sand only.

Agreement between the saturation profiles of the three techniques is quite good. The average difference between curves is less than 5% saturation, with the greatest deviation being approximately 10% saturation. These differences are encountered at the inflection points and in zones of low saturation. With respect to the inflection points, the X ray and light techniques tend to overestimate relative to the gamma densitometer technique, while the X ray tends to initially underestimate and then overestimate saturation relative to the light technique. These discrepancies may be due

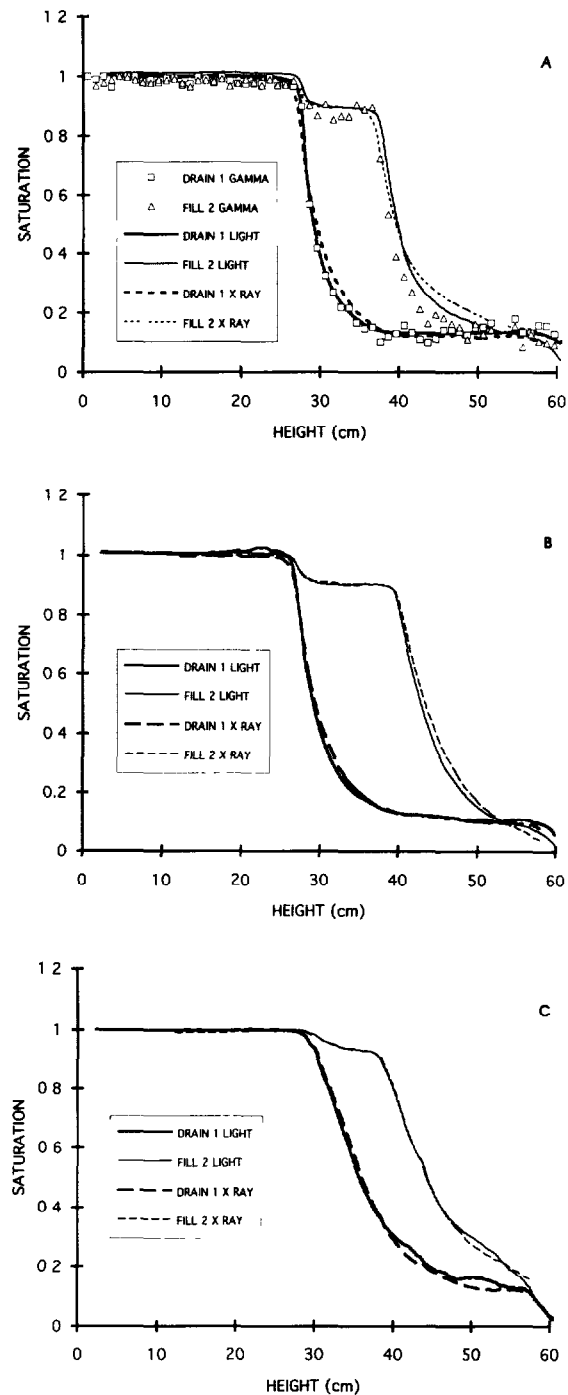


**Figure 3.** Saturation as a function of chamber height as measured by the X ray, light, and gamma techniques. The drain 2 sequence has been omitted from each profile for the sake of clarity. (a) Saturation profile for the 0.42- to 0.30-mm sand. (b) Saturation profile for the 0.59- to 0.21-mm sand. (c) Saturation profile for the 0.84- to 0.149-mm sand.

in part to temperature, orientation, and alignment changes of the chamber during transport between the light, X ray, and gamma facilities (discussed below). Other sources of discrepancies may include light and X ray scatter, each of which are enhanced in areas of high moisture contrast (discussed below).

To aid in the interpretation of the saturation profiles we

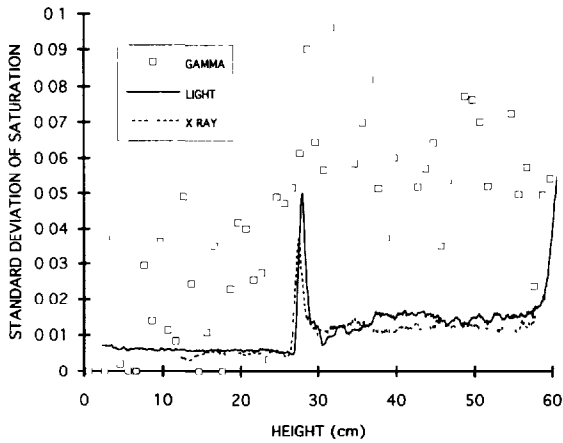


**Figure 4.** Standard deviation profile as a function of chamber height as measured by the X ray, light, and gamma techniques. Shown here are the profiles for the drain 1 series of the 0.42- to 0.30-mm sand.

also have plotted the standard deviation as a function of chamber height for the drain 1 series of the 0.42- to 0.30-mm sand (Figure 4). These profiles were selected because they are representative of the behavior noted for the other series and sands tested. On the basis of this comparison, grey level profiles for the three techniques are within one standard deviation of each other. Also of interest is the increase in the standard deviation that occurs at the inflection point between fully and partially saturated conditions. This variance is not solely an artifact of the measurement techniques but is more of an indication of the variability in the saturation field itself. Because the light and X ray techniques are applied at a spatial resolution of approximately 3 times the mean grain size, we are actually capturing ganglia (pore clusters) scale variation.

Our third comparison investigates the X ray and light transmission saturation fields point-by-point throughout the entire domain. Absolute-difference images are calculated to visualize discrepancies between the saturation fields measured by each technique. Two absolute-difference fields, drain 2 for the 0.59- to 0.21-mm sand, and fill 2 for the 0.42- to 0.30-mm sand, are shown in Plates 2a and 2b. These fields were selected because they represent the best and worst agreement between the two techniques within the nine saturation fields analyzed. Bright red represents differences of 9% saturation, grading to black, which represents a zero absolute difference. The isolated bright spots in the error fields result from impurities (metallic mineral grains) in the sands that corroded over time (because of the KI solution), influencing light but not X ray transmission. The distinct vertical red band in Plate 2b results from spatial heterogeneity in the light source intensity field, which differed between the X ray and light images as is discussed below.

## 5. Discussion of Error

Three categories of error influence the results reported in this section. The three are those resulting from the comparison experiments, those intrinsic to the measurement techniques (i.e., precision), and those due to assumptions implicit in the conceptual models used to calculate saturation from the X ray and light data.

### 5.1. Experimental Error

Errors due to the comparison experiments stem from the need to move the experiment between three test facilities and to use a concentrated KI solution. During transport, temperature variations of up to 20°C were experienced which caused expansion and contraction in the trapped air within the bottom supply manifold. In addition to slight chamber tipping while negotiating stairways and doors, high winds also were experienced while the experiment was carried the 0.5-km distance between facilities. The temperature and tipping problems were greatest during testing of the 0.42- to 0.30-mm sand, in which the greatest discrepancy in the saturation fields at the inflection points occurred. At each facility the experiment also had to be aligned properly with respect to the source and detector. Perfect alignment was impossible, resulting in a misalignment of about 1–2 mm each time the chamber was moved. Such misalignment can cause errors of up to 5% saturation where moisture conditions are rapidly varying. Other errors occurred because of corrosion of metallic impurities by the KI solution that caused localized discrepancies of the order of 9% saturation.

### 5.2. Error Intrinsic to the Measurement Techniques

To evaluate the precision of the imaging techniques, nine pairs of repeated images (X ray and light) were acquired during tests performed with the 0.42- to 0.30-mm sand: three images each from the drain 1, fill 2, and drain 2 equilibrium saturation fields. Each of the raw images was adjusted and scaled; then the paired images were subtracted to quantify the absolute differences between the repeated images. Two absolute-difference fields are shown in Plates 3a and 3b which represent the best and worst agreement achieved. Red represents an absolute difference of 4% saturation, grading to black, which represents a zero absolute difference. Measurement precision was found to be consistent regardless of the technique or imaging sequence. Given that both techniques make use of the same digital imaging system, similarity in the precision of the X ray and light techniques is expected.

Characteristics of the differences between images used in the precision analysis indicate two sources of error. One, which gives rise to the randomly distributed error, is attributed to video signal noise. On average, this noise is responsible for errors of the order of 1.5% saturation, which can be reduced with more sophisticated and expensive, nonvideo-based digital cameras. The other source of error gives rise to differences of a more structured nature, as apparent in the upper right-hand side of Plate 3b. Such errors arise from slight variations in the source field that are not uniformly distributed across the full imaging plane. Again, the error is relatively minor, with maximum variation of 4% saturation. Although the X ray and light images are adjusted to account for average changes in the source intensity field, it is impossible to correct, by image manipulation, for localized spatial variations that are not uniformly distributed throughout the imaging plane. This problem, demonstrated in both Plates 2b and 3b, is due to differences in the uniformity of the emitted light behind the porous slab or X ray film. Variations in the light source occur each time the system is turned on and off. Also, the output of the bulbs is a function of temperature and thus light source ventilation and room temperature. These tests were conducted with a feedback circuit on the light source to stabilize its spatially integrated

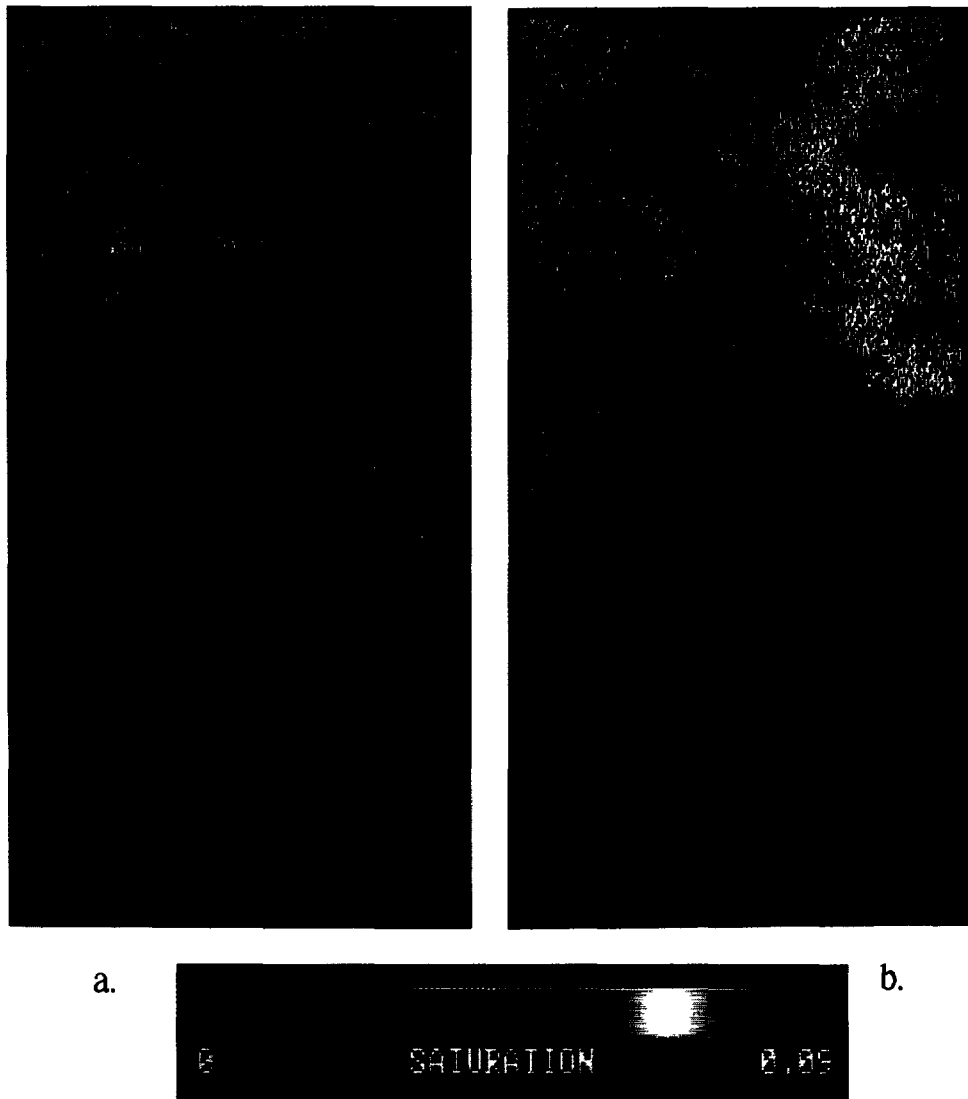


**Plate 2.** Direct comparison of the saturation fields as measured by the X ray and light techniques. Two absolute-difference fields are shown, (a) drain 2 for the 0.59- to 0.21-mm sand and (b) fill 2 for the 0.42- to 0.30-mm sand, representing the best and worst agreements, respectively. Bright red represents areas with the greatest absolute difference (9% saturation), grading to black, which represents a zero absolute difference.

output. Control on individual bulbs within the bulb bank is possible and should allow stabilization of the light source intensity field to minimize associated error.

### 5.3. Error Related to Assumptions in Conceptual Models

The third source of error is due to simplifications in our conceptual models for calculating liquid saturation from the X ray and light intensity data. In deriving equation (6), we have neglected the polychromatic nature of the X ray source with the argument that the chamber and sand tend to narrow the X ray energy spectrum effective in imaging media saturation. Given the good agreement of the X ray data with the light, gamma, and gravimetric data, treatment of the X ray spectrum effective in imaging as monochromatic (as assumed by Lambert's law) appears suitable for application to the systems investigated here. The suitability of the simple, one-parameter, physically based relation between

saturation and emitted light intensity (equation (11)) to model the investigated porous systems also appears appropriate. One of the purposes for using three different sands (with broadening grain size distributions) was to evaluate the effect of pore size distribution on saturation calculations for the light technique. Comparison of the wetting and drainage curves as measured by the X ray and light techniques (Figure 3) shows little difference regardless of the grain size distribution, thus indicating the robustness of (12).

An additional source of error is the neglect of X ray and light scatter. X ray and light scatter effects, enhanced in zones of high moisture contrast, tend to smooth out an otherwise sharp contrast. As such, these effects are most important in zones of high contrast. Absolute error was found to be less than 10% saturation in regions of high contrast, with at least 5% attributable to equipment misalignment and experiment movement, as was discussed previ-

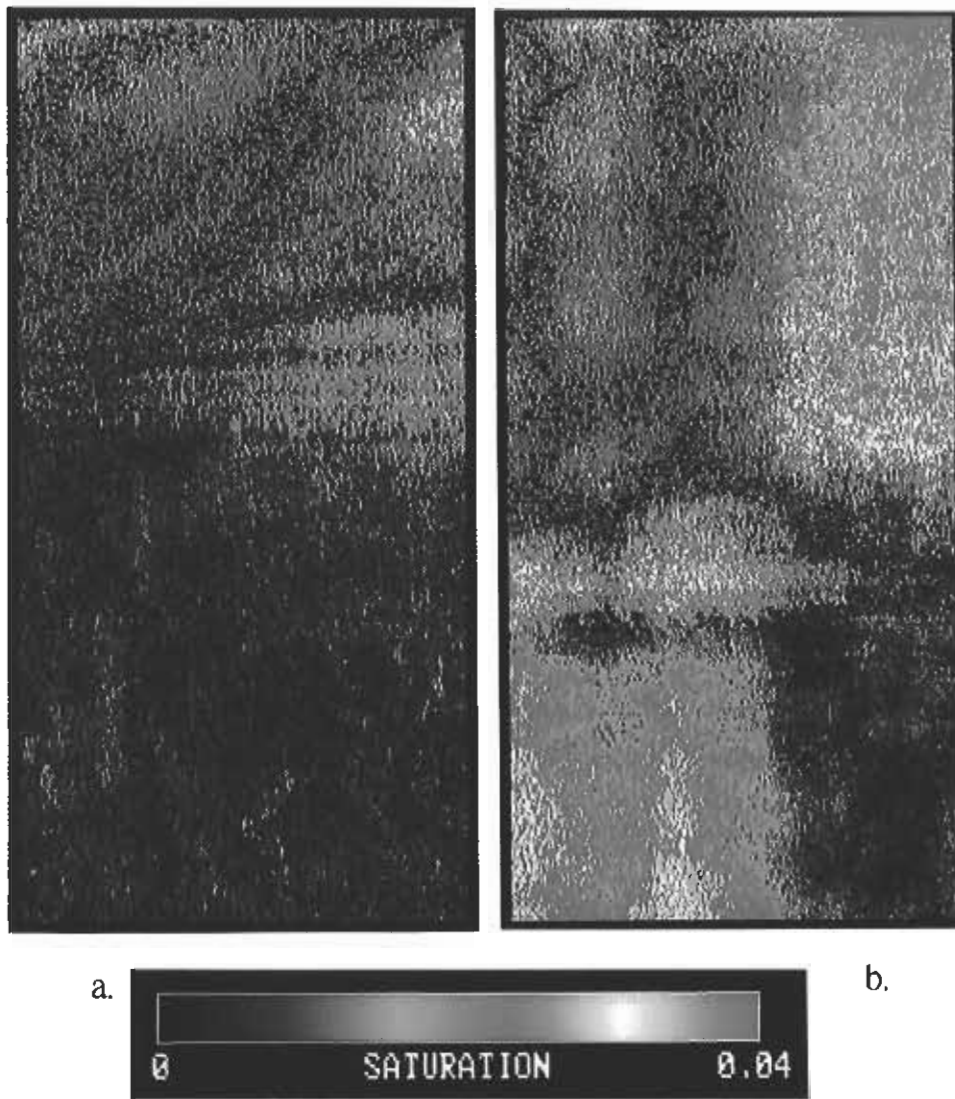


**Plate 3.** Images used in evaluation of technique precision. Two absolute-difference fields are shown, (a) drain 2 and (b) drain 1 series of the 0.42- to 0.30-mm sand, representing the best and worst agreements, respectively. Bright red represents the greatest absolute difference (4% saturation), grading to black, which represents a zero absolute difference.

ously. However, given that each of the energy transmission techniques used here suffers from scatter effects to some extent, further work needs to be performed to both characterize scatter and incorporate its physics in the algorithms used to calculate saturation.

## 6. Conclusions

Two high-resolution techniques for measuring two-dimensional transient saturation fields in thin-slab systems have been developed, demonstrated, and compared. These techniques have the advantage that in the time it takes to measure a single point by one of the traditional techniques, an entire image consisting of hundreds of thousands of points can be acquired by the X ray and light techniques. However, as with any measurement technique, there are limitations that must be considered, such as the requirement to use a

nonopaque medium for the light technique and the need for a more highly X ray absorbing liquid than water for the X ray technique.

On the basis of the results presented in this paper, both the X ray and light techniques are capable of providing quantifiable saturation information. Comparisons with gravimetric and gamma densitometry methods show the data to agree on average within 5% saturation. The high resolution of these techniques coupled with the quality of data that they yield makes these techniques valuable tools for investigating unsaturated flow phenomena. In particular, these techniques greatly facilitate investigations involving transient conditions as well as investigations involving heterogeneous and/or fractured media [e.g., *Glass and Tidwell, 1991; Foltz et al., 1993*]. Although the possibility is not explored in these experiments, both techniques are capable of measuring solute concentration fields and bulk density fields at a

resolution comparable to that demonstrated in the comparison studies presented. Applications of the techniques to multiphase systems involving fluids other than air and water are also straightforward.

**Acknowledgments.** We would like to acknowledge a number of people who were instrumental in this research. Lee Orear helped in the development of the optical system and numerous software tools, Craig Ginn was responsible for design and fabrication of much of our test equipment, Ragimera Amato helped in data collection and reduction, Deanna Sevier aided in the collection of our X ray images, and Anthony Russo allowed us access to the gamma facility and gamma data reduction programs. We would also like to acknowledge Bruce Hansche and Charles Kelsey (University of New Mexico), whose advice proved very valuable in the development of the X ray imaging technique. Robert Glass also acknowledges support of EPA grant R81-2919-01-0 and the help of J. Throop of Cornell University during his initial development of the light transmission technique in 1988. The majority of this work was supported by the U.S. Department of Energy, Office of Civilian Radioactive Waste Management, Yucca Mountain Site Characterization Project Office, under contract DE-AC04-76DP00789.

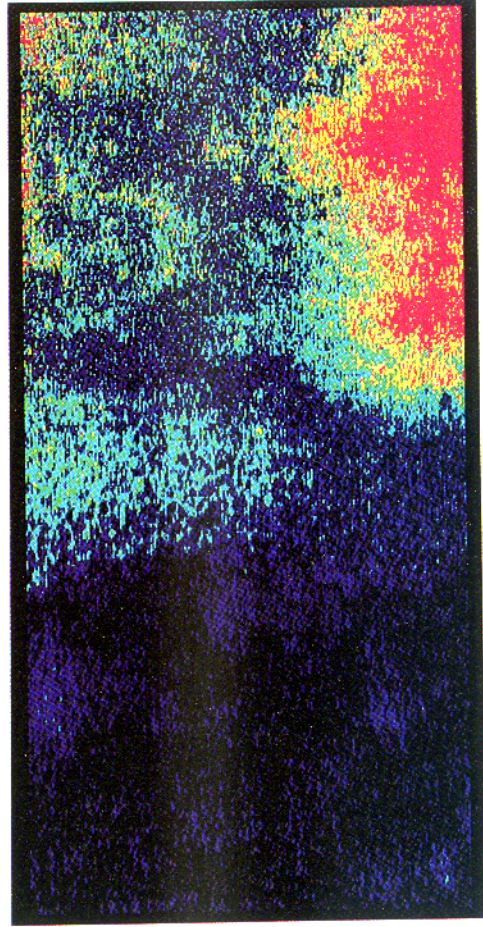
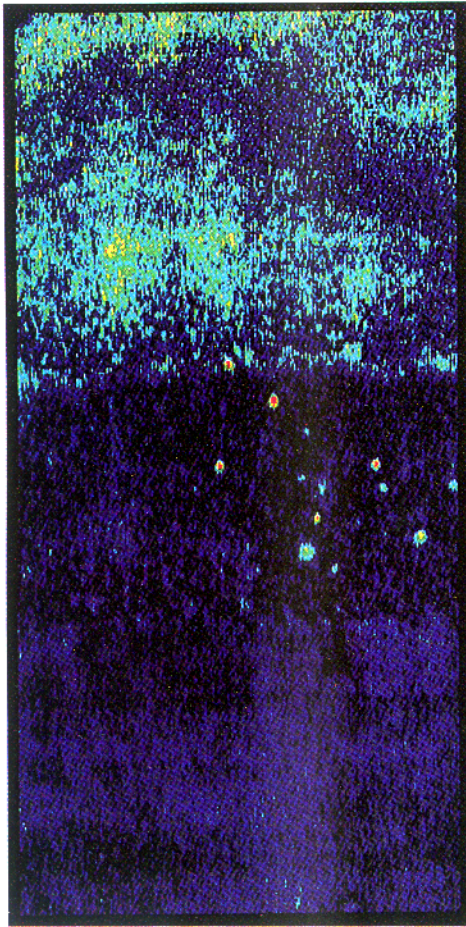
## References

- Anderson, S. H., C. J. Gantzer, J. M. Boone, and R. J. Tully, Rapid nondestructive bulk density and soil-water content determination by computed tomography, *Soil Sci. Soc. Am. J.*, 52, 35-40, 1988.
- Brown, J. G., *X-Rays and Their Applications*, Plenum, New York, 1966.
- Crestana, S., S. Mascarenhas, and R. S. Pozzi-Mucelli, Static and dynamic three-dimensional studies of water in soil using computed tomographic scanning, *Soil Sci.*, 140, 326-332, 1985.
- Daily, W., and A. Ramirez, Evaluation of electromagnetic tomography to map in situ water in heated welded tuff, *Water Resour. Res.*, 25, 1083-1096, 1989.
- Foltz, S. D., V. C. Tidwell, R. J. Glass, and S. R. Sobolik, Investigation of fracture-matrix interaction: Preliminary experiments in a simple system, paper presented at 4th Annual International High-Level Radioactive Waste Management Conference, Am. Nucl. Soc., Las Vegas, Nev., 1993.
- Gardner, W. H., Water content, in *Methods of Soil Analysis*, edited by A. L. Page, R. H. Miller, and D. R. Kenney, *Am. Soc. Agron.*, 493-541, 1982.
- Glass, R. J., and V. C. Tidwell, Research program to develop and validate conceptual models for flow and transport through unsaturated fractured rock, paper presented at 2nd Annual International High-Level Radioactive Waste Management Conference, Am. Nucl. Soc., Las Vegas, Nev., 1991.
- Glass, R. J., T. S. Steenhuis, and J.-Y. Parlange, Mechanism for finger persistence in homogeneous, unsaturated, porous media: Theory and verification, *Soil Sci.*, 148, 60-70, 1989a.
- Glass, R. J., T. S. Steenhuis, and J.-Y. Parlange, Wetting front instability, 2, Experimental determination of relationships between system parameters and two-dimensional unstable flow field behavior in initially dry porous media, *Water Resour. Res.*, 25, 1195-1207, 1989b.
- Hoa, M. T., A new method allowing the measurement of rapid variations in water content in sandy porous media, *Water Resour. Res.*, 17, 41-48, 1981.
- Kaelble, E. F., *Handbook of X-Rays*, McGraw-Hill, New York, 1967.
- Kravchuk, E. M., and E. A. Strashkevich, Sensitivity and accuracy of the roentgenoscopic method of determining moisture content in a porous body, *J. Engl. Phys.*, Engl. Transl., 25, 859-863, 1973.
- Latorre, V. R., and H. D. Glenn, Microwave measurements of the water content of bentonite, paper presented at 2nd Annual International High Level Radioactive Waste Management Conference, Am. Nucl. Soc., Las Vegas, Nev., 1991.
- Matzkanin, G. A., and R. F. Paetzold, Measuring soil water content using pulsed nuclear magnetic resonance, *ASAE Tech. Pap.* 82-2619, Am. Soc. Agric. Eng., St. Joseph, Mich., 1982.

R. J. Glass and V. Tidwell, Geoscience Center, 6115, MS 1324, Sandia National Laboratories, Albuquerque, NM 87185. (e-mail: rjglass@Sandia.gov; vtidwell@Sandia.gov).

(Received February 22, 1993; revised April 4, 1994; accepted April 6, 1994.)

Plate 1.

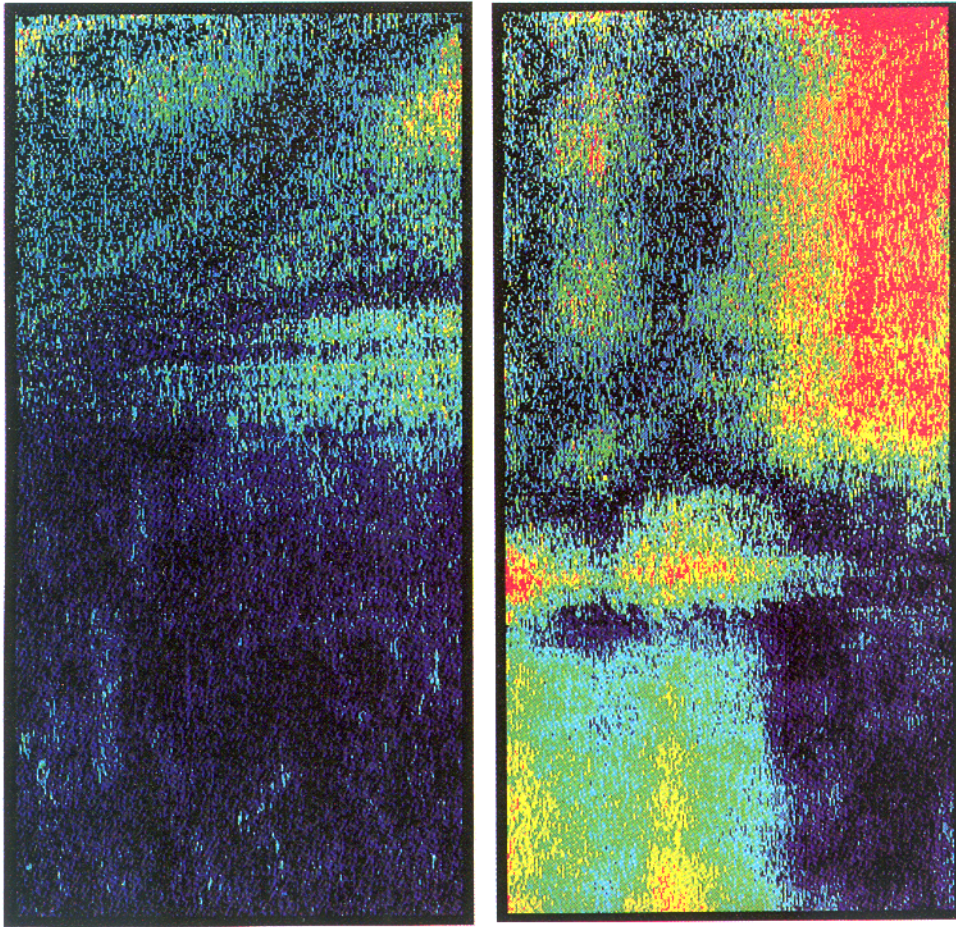


a.



b.

Plate 2.



a.



b.